International Journal of Computer Information Systems and Industrial Management Applications.
ISSN 2150-7988 Volume 5(2013) pp. 001–010

A Retinex theory based points sampling method

Yitian Zhao, Yonghuai Liu, Ran Song and Min Zhang

Department of Computer Science,
Aberystwyth University,
Aberystwyth, Ceredigion, United Kingdom, SY23 3DB
yyz10@aber.ac.uk

Abstract: **To accelerate the processing for integration, registration, representation and recognition of point clouds, it is of growing necessity to simplify the surface of 3-D models. This paper proposes a Retinex theory based points sampling method and the effectiveness of the sampling results are demonstrated by the point cloud registration and mesh simplification. The points sampling method considers both the local details and the overall shape of the model. The local details are captured by a graph-based segmentation, while for the overall shape, the approach voxelizes the model and samples points in terms of the entropy of the shape index of vertices in voxels. We present a number of results to show that the method significantly simplifies the surface without losing local details and global shape. The effectiveness of this method is finally demonstrated by point cloud registration results of overlapping range images and mesh simplification errors.**

Keywords: Retinex, sampling, registration, point cloud, local, global.

I. Introduction

Laser range scanners have become more and more popular for 3D measurement. The output of laser range scanners is a set of structured data points with or without reflectance strength information, depicting the reflectance characteristics of the 3D objects of interest. The structured data points can easily be triangulated and rendered as range images. However, most of the range scanners usually generate huge amounts of data points. A complete model could contain millions of points and often leads to expensive processing time. This creates facing great challenges, such as storage, editing and transmission. Thus efficient and accurate simplification of point cloud is necessary and the simplified points cloud has become a powerful alternative to the original data. The simplified points usually can be sampled through a combination of various mesh operations, such as feature points detection and segmentation. The sampled points can accelerate either the display or processing of the large 3D data. In the point sampling, it is important to choose the representative and distinctive points. The points must have some significant properties, such as invariant to affine transformations and robust to the noise and robust to different tessellations. Points sampling is necessary to select distinctive points on a model and thus gains efficiency in their processing. Some tasks that benefit from this capability are object registration, integration, simplification, retrieval, texture mapping, and deformation.

In the past years the evaluations of point feature detectors in the matching, recognition or texture classification have been proposed. The popular Harris corner detector [4] is improved upon Moravec's corner detector by investigating local auto-correlation function of the signal which reflects the local distribution of gradient directions in the image. Shi-Tomasi feature detector [5] is strongly based on the Harris detector. The difference between them is that this detector computes the minimum of the absolute values of the eigenvalues of the structural tensor. SIFT detector [6] is based on the algorithm developed by Lowe in order to detect the scale-invariant image features, which consists of keypoints detecting and tracking. Lo [8] presented a 2.5D SIFT algorithm that extracted robust feature points on range images, which is by concatenating the histogram of the range surface topology types. However, these methods have two drawbacks: the limited repeatability of a feature point detector and the drift of the feature point.

Nehab et al. [19] presented a stratified sampling strategy for 3D data that is a technique to generate evenly spaced samples by subdividing the sampling domain into non-overlapping parts and sampling independently from each part. Osada et al. [9] proposed a method which is uniformly sampled on a triangulation mesh. This sampling approach basically generated random sample points in the randomly picked triangles with equal probability per unit area. Turk [10] described a sampling approach that started from an uniform sampling of the mesh and placed a charged particle at each sampled position, where the particles are allowed to repel each other until equilibrium is reached during the constraining on the remain surface.

Moreover, the techniques of interest points detection is expanded to the human visual system area: Itti et al. [28] created a computational model of saliency-based spatial attention derived from a biologically plausible architecture. The saliency maps for features of luminance, color and orientation at different scales were computed. Hu et al. [29] proposed saliency maps by thresholding the color, intensity and orientation maps. In this method, the histogram entropy thresholding analysis was employed. More recently, the selection of interest points is exploited to the notion of saliency in the 3D domain. Lee et al. [30] defined a mesh saliency for the mesh simplification. This approach is using a center-surround operator on the local curvature as the discrimina-

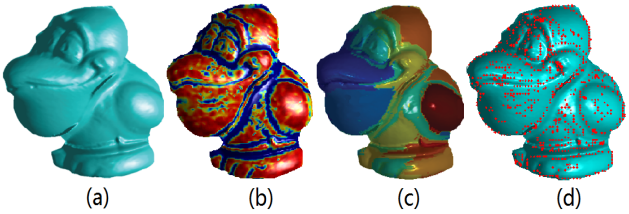

Figure. 1: The results at different stages of the proposed algorithm: (a) Input model;(b) Retinex applied on the shape index. Red area presents the smooth region and blue presents the concave/convex area; (c) Segmentation. Different color presents different regions on the surface; (d) Points sampled

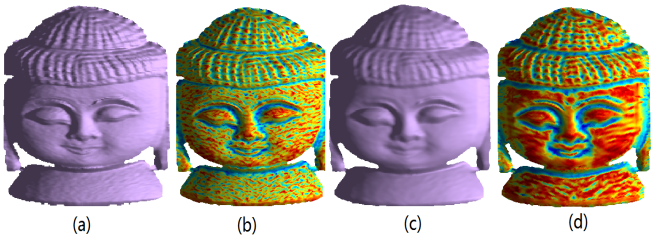

Figure. 2: (a) Original mesh. (b) Original mesh colored by shape index. (c) Mesh smoothed by non-local means filter. (d) Smoothed mesh colored by shape index

tive feature. Pauly et al. [31] presented a multi-scale technique for extracting line-type features on a point-sampled geometry. A measure of surface variation and persistence of feature-points over different scales was used. Shilane et al. [32] defined distinction as the retrieval performance of a local shape descriptor. After a training phase, the retrieval performance of each descriptor has been evaluated and only the most distinctive are retained. Frome et al. [33] introduced regional point descriptors, which contain 3D shape and harmonic shape context. This approach extracts the points by random sub-sampling the whole set of points. Owing to its efficiency of visual persuasion in traditional art and technical illustrations, visual saliency has now been widely used in many computer graphics applications, including saliency guided shape enhancement [34]. Miao et al. [35] proposed a normal perturbation technique to enhance the visually salient features of 3Dshapes explicitly. This method demonstrate that saliency guided shading scheme can improve the depiction of the underlying shape and the perception of its salient features.

The Retinex theory is originally proposed by Land and McCann in 1971 [18]. The goal of the Retinex method is to decompose a given image into a reflectance image and an illumination image. The benefits of such decomposition include the ability to remove the illumination effects, enhance the image which includes spatially varying illumination and correct the colors in the image by removing illumination induced color shifts [12]. Many applications have adapted the Retinex algorithm, such as image editing, multi-spectral image fusion and high dynamic range compression. Jobson et al. [15] proposed a single scale Retinex (SSR) that employs a simple linear filter with Gaussian kernel. He also extended SSR to muliti scale Retinex (MSR) [16] by combining several low-pass filtered copies of the logarithm of Retinex image using different cut-off frequencies for each low-pass filter. Gross and Brajovie [14] used an anisotropic filter to reduce the halo effects to some extent. Self quotient image (SQI) has been proposed resulting in impressive improvement of performance in dealing with illumination variation problem. Elad [12] introduced an algorithm that uses two specially tailored bilateral filters. The first filter evaluated the illumination and the other calculated the reflectance.

This paper proposes a new Retinex theory based points sampling method and it consists of five phases: Mesh filtering, Retinex, segmentation and sampling. A bilateral filters based Retinex method is then introduced that uses segmentation to extract the local details. Some experiments are demonstrated and the effectiveness of this method is finally demonstrated by different registration and simplification methods.

II. Algorithm

In this section we propose an algorithm to detect and sample the meaningful points on 3D surface. The proposed method is combined four steps: (1)Mesh filtering. (2)Retinex decomposition. (3)Segmentation. (4)Points sampling. Fig. 1 shows the structure of our method.

A. Mesh filtering

The acquired data of the 3D model usually contains imaging noise from various sources, such as scanning noise. It is very important to remove the noise while preserving the underlying sampled surface, in particular its fine features. In order to produce more accurate results, this paper employs the Non-local mean filter [36] which is a simple but efficient method to smooth the polyhedral surface and improve the appearance of the object. Basically this algorithm reduces the high frequency surface information and tends to flatten the surface.

The basic idea of non-local mean filter is that it assumes an extensive amount of self similarity is contained in an image. Thus, similarity is measured based on the geometrical configuration in the whole neighborhood instead of measured based on every single pixel. Let I be a given image. Based on a weighted average of all pixels in its neighborhood Θ, the value $I'(u)$ at pixel u can be estimated by

$$I'(u) = \frac{\sum_{v\in\Theta} \psi(u,v) I(v)}{\sum_{v\in\Theta} \psi(u,v)} \tag{1}$$

where the weight $\psi(u,v) = exp(-\frac{\|\Theta_u - \Theta_v\|^2_{2,a}}{d^2})$ is computed by the similarity of the Gaussian neighborhood between pixels u and v. Θ_u is a square neighborhood centered at pixel u. a is the standard deviation of the Gaussian kernel and d is the delay parameter.

In this section, the non-local means filter is extended to process the shape index of a 3D mesh. Koenderink [17] has suggested that the shape index ϑ could give a simple measurement of the local shape. It can present the flat concave

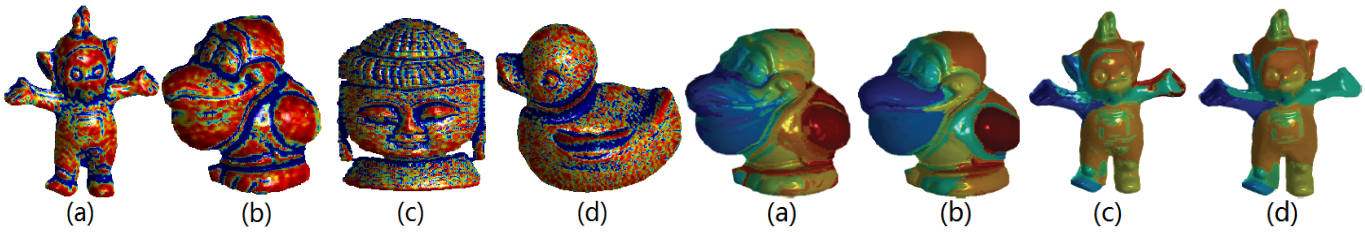

Figure. 3: Retinex applied on the models. (a)tubby; (b)bird; (c)buddha; (d)duck

Figure. 4: Odd column: Graph-based segmentation without Retinex applied; Even Column: Graph-based segmentation with Retinex applied

and convex rejoin significantly. The shape index can be estimated by the principal curvature:

$$\vartheta = \frac{2}{\pi} \arctan \frac{k_2 + k_1}{k_2 - k_1} \tag{2}$$

where k_1 and k_2 are the principle curvature which can be calculated by Taubin [20].
The non-local means filter can be applied to diffuse the shape index field as the shape index can be considered as a signal defined over its domain. In order to determine the given vertex's similarity with the neighborhood, the B-spline [37] algorithm is employed. The similarity between neighborhoods in a mesh can be measured by computing the corresponding vertex on the surface, because the underlying control net is topologically similar to the image grid structure when using B-spline surfaces:

$$Q(u,v) = \sum_{i=1}^{4}\sum_{i=1}^{4} B_{i,j} N_(i,k)(u) M_{j,l}(v) \tag{3}$$

where $B_{i,j}$ are control points and in their natural ordering, $N_{i,k}(u)$ and $M_{j,l}(v)$ are the B-spline basic function in the biparametric u and v directions, respectively. We use the 2-ring vertices of v_i as the input data, then project the input data points and scale them to the range [0,1].
Fig. **??** shows the result of the proposed mesh filtering method on range image data. The result shows that the method not only smoothes the surface, but also retains visually meaningful details.

B. Retinex based decomposition

Most 3-D images are captured by cameras and scanners, thus they usually contain imaging noise from various sources or the images are visually undesirable. Retinex theory [11] deals with the removal of unfavourable illumination effects from images in order to improve their quality. The theoretic foundation of the Retinex is that an image $I(x,y)$ is regarded as a product $I(x,y) = L(x,y) * R(x,y)$, where $L(x,y)$ is the illumination image and $R(x,y)$ is the reflectance image. Generally, $L(x,y)$ is determined by the illumination source and $R(x,y)$ is determined by the characteristics of the imaged object. This paper presents a Retinex theory based bilateral filter to compensate the illumination for segmentation by using the shape index image. The illumination L is estimated by a shift invariant Gaussian filter. The bilateral filtering can be described as follows:

$$h(x) = k^{-1}(x) \int_{-\infty}^{\infty}\int_{-\infty}^{\infty} f(x_n) g(x_n, x) s(f(x_n), f(x)) d(x_n) \tag{4}$$

where the normalization

$$k(x) = \int_{-\infty}^{\infty}\int_{-\infty}^{\infty} g(x_n, x) s(f(x_n), f(x)) d(x_n) \tag{5}$$

where $g(x_n, x)$ measures the geometric closeness between the center of neighbourhood x and a nearby pixel x_n and it can be expressed by Eq. 6.

$$g(x_n, x) = e^{-\frac{1}{2}(\frac{d(x_n,x)}{\sigma_d})^2} \tag{6}$$

where $d(x_n, x)$is the Euclidean distance between x_n and x, σ_d denotes the geometric spread chosen based on the desired amount of low-passing filtering. $s(f(x_n), f(x))$ measures the photometric similarity between the x and x_n. The similarity function s can be defined as:

$$s(f(x_n), f(x)) = e^{-\frac{1}{2}(\frac{d(f(x_n),f(x))}{\sigma_r})^2} \tag{7}$$

where $d(f(x_n), f(x))$ is the distance between the two shape index values $f(x_n)$ and $f(x)$. σ_d is the photometric spread in the image range that is set to achieve the desired amount of combination of shape index values. By estimating the illumination L, the reflectance image R is defined as follows:

$$R(x,y) = log(I(x,y) + 1) - log(L(x,y) + 1) \tag{8}$$

where $I(x,y)$ is the input shape index image which is estimated in the previous section and $L(x,y)$ is the illumination image. Fig. 3 illustrates some examples by applying Retinex theory. It is clearly shown that this method can distinctly recognize the flat, concave and convex regions.

C. Segmentation

In order to sample the local points which could represent the local details, segmentation is an important step. Felzenszwalab [13] introduces an efficient graph-based image segmentation based on pairwise region comparison. It produces segmentations that obey the global properties of being not too coarse and not too fine by using a specific region function. In this paper, the graph-based segmentation is employed to segment the reflectance image which is estimated by Eq. 8. The

Figure. 5: Points sampled on model tubby1-2, bird1-2, buddha1-2 and duck1-2 with simplification rate 90%. Top row: local points sampled. Bottom row: combined global and local sampled points in an appropriate combination rate.

pairwise comparison predication is defined by Eq. 9 in order to evaluate whether or not there is evidence for a boundary between two regions in a segment.

$$D(R_1, R_2) = \begin{cases} true & \text{if } Dif(R_1, R_2) > MInt(R_1, R_2) \\ false & \text{otherwise} \end{cases} \tag{9}$$

where $Dif(R_1, R_2)$ denotes the difference between two regions R_1 and R_2:

$$Dif(R_1, R_2) = \min_{v_i \in R_1, v_j \in 2, (v_i, v_j) \in E} w(e) \tag{10}$$

where $w(e) = \|Int(v_i) - Int(v_j)\|$ is the corresponding weight of the edge that was estimated by the shape index. $MInt(R_1, R_2)$ denotes the minimal invariant difference:

$$MInt(R_1, R_2) = \min(Int(R_1) + \tau(R_1), Int(R_2) + \tau(R_2)) \tag{11}$$

where the invariants difference is defined as

$$Int(R) = \max_{e \in MST(R,E)} w(e) \tag{12}$$

the MST is the minimum spanning tree, τ is the threshold function which controls the degree to which the difference between two components must be greater than their internal differences in order for there to be evidence of a boundary between them (D to be true). The segmentation obeys the properties of being neither too coarse nor too fine, according to the following definitions:

Definition 1: A segmentation S is too fine if there are pairs of region $R_1, R_2 \in S$ where no evidence for a boundary exists between them.

Definition 2: A segmentation S is too coarse if there exists a proper refinement of S that is not too fine.

The most important reason to implement the segmentation in this method is that it can perceptually capture important grouping or regions that often reflect global aspects of the image. Fig. 4(a) and (c) show the results of the graph-based segmentation without Retinex applied. It is clearly shown that the $bird$ and $tubby$ models have been over-segmented and need to be improved. Fig. 4(b) and (d) show the results of the graph-based segmentation with Retinex applied, the segmented results are significantly improved, where the over-segments are merged or removed.

D. Points sampling

1) Local points sampling

Because the surface has been segmented into a limited number of regions, the feature points can be selected from each region. The selection criterion selects points from each segment by thresholding the absolute shape index values. The top row of Fig. 5 shows the results after local point sampling where only a few points are selected in the flat region, whereas more are selected in the regions with more detail, such as the eyes of the $bird$ and $tubby$. The points that have been sampled by the local sampling algorithm sometimes focus too much attention on the local details and overlook the overall shape. Hence, the selected points may not represent the model shape well and might miss meaningful parts of the shape. In order to address the problem, global sampling is applied in this paper.

2) Global points sampling

In this section, a modified stratified point sampling method [19] is employed. This algorithm voxelizes the surface and selects one or more points from each voxel based on the entropy of the shape index of vertecies and restricted to the original model's surface. The entropy measures how the shape index of vertices in a voxel varies. The larger the variation, the larger the entropy, the more detail the voxel contains. Thus the entropy can be used to guide the points sampling. This algorithm is basically divided into four steps:

- The first step voxelizes the model by the bounding boxes and the model can be divided into several sub boxes. The resolution of the voxelization is specified by the user.

- Based on the histogram of shape index, the entropy can

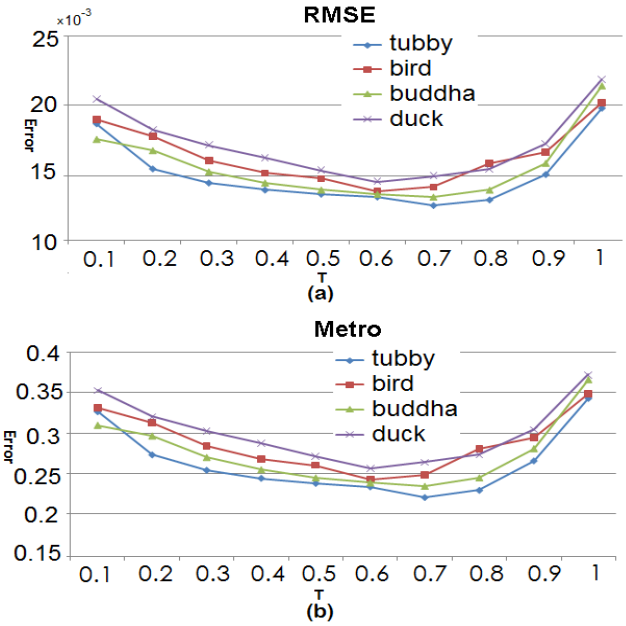

Figure. 6: The evolution of the RMSE errors (a) and Metro errors (b) with different parameter T, tested on tubby, bird, buddha and duck.

be calculated by

$$H(X) = \sum_{i=1}^{n} - P(r_i) * log_2(P(r_i)) \qquad (13)$$

where $P(r_i)$ is the probability of vertex r_i in a local voxel, n denotes the total number of the vertices.

- The third step chooses one or more points from each sub box based on the estimated entropies. Normally, the maximum entropy is always chosen.

- The minimum distances between the samples are used to address the possibility that the generated samples are close to the boundary between two or more adjacent voxels which might be too close to each other.

3) Points combination

In order to achieve a better simplification result, the sampled local and global points are combined. By denoting the points from local sampling as L_s and the points from global sampling as G_s, the simplification approach is defined as follows:

$$SIM = T \cdot L_s + (1 - T)G_s \qquad (14)$$

where T denotes the weight of local sampling and $T \in [0, 1]$. If T is small, the method presents the global shape well, but may lose a lot of local shape information. When T is large, the local shape could be represented well but the global shape may be destroyed. So an appropriate value for T needs to be defined. Based on the evolution of the simplified mesh errors which is introduced in [1], we define $T = 0.65$ in this paper. The bottom row of Fig. 5 shows the sampled points which are generated by combining the global and local sampled points with an appropriate combination rate. It can be seen that the sampled points have more potential to represent the local details and global shape.

Table 1: RMSE ($*10^{-3}$) and Metro Errors measured for some models using QSlim and SSim

Model	Simp. rate	RMSE QSim	RMSE SSim	Metro QSim	Metro SSim
tubby	50%	14.61	12.11	0.26	0.23
	90%	17.20	13.32	0.31	0.27
	95%	19.73	15.30	0.33	0.32
bird	50%	16.81	9.45	0.35	0.21
	90%	16.22	11.02	0.41	0.33
	95%	21.03	11.63	0.50	0.39
buddha	50%	16.33	10.00	0.47	0.33
	90%	17.85	12.12	0.58	0.42
	95%	23.28	13.39	0.61	0.51
duck	50%	12.44	11.16	0.21	0.19
	90%	15.33	14.21	0.30	0.23
	95%	18.46	17.34	0.37	0.31
lobster	50%	21.54	16.53	0.45	0.39
	90%	25.42	18.21	0.57	0.42
	95%	28.32	21.24	0.67	0.53

III. Experimental results

Neither the range image segmentation nor the range image points sampling has the groundtruth, so the sampling accuracy cannot be determined. To solve this problem, mesh simplification and point cloud registration approaches are applied. The simplification and registration errors indicate the efficiency of the proposed point sampling method.

A. Simplification

The sampled points also can be seem as a simplifed point cloud. The simplifed point cloud could be triangulated into mesh easily. The measured errors between the simplified and orginal mesh always present the effectiveness of the simplification. In order to evaluate the effect of the simplification criteria, our algorithm (SSim) has been compared with the geometric QSlim [39] algorithm which uses the best half-edge collapse. The QSlim algorithm was chosen because of the high-quality of its approximations and its code is freely available. Although the QSlim algorithm was proposed some time ago, it still achieves competitive results. For the comparative study, a publicly available range image database hosted by the signal analysis and machine perception laboratory at Ohio State University was used [40]. To this end, several experiments with meshes of differing complexities were performed. All models were simplified on a computer with Intel Core 2 Duo CPU E8400, 3.00GHz. The visual and geometric errors are the differences between the original mesh and simplified mesh, which were measured using root mean squared error(RMSE) and Metro error. RMSE is used as an efficient measurement in the mesh simplification. In the mesh comparison tool named Metro [38], the Hausdorff distance between two polygonal meshes was measured:

$$E_{(S,S')} = \sqrt{\frac{1}{AREA} \int d(p, S')^2 ds} \qquad (15)$$

where the S is an orientable surface, $AREA$ is the area of the surface S and $d(p, S')$ is the distance between a point p

Figure. 7: Simplification by using QSim and SSim and simplification rate 90% on tubby, bird, buddha, duck, angel, lobster, frog and valve. Top column: Original; Middle column QSim; Bottom column: SSim

of S and S'.

In order to obtain an efficient fusion of global sampled points and local sampled points, it is necessary to determine an appropriate value for the parameter T. Fig. 6 compares the SSim errors of $tubby, buddha, bird$ and $duck$, which were measured by RMSE and Metro for different values of T under the condition that the simplification rate is 90% (it means 90% of vertices are removed). For $T = 0$, all the points are selected globally and it obtains a large error. For $T = 1$, only local points are selected without the global shape information and as shown in Fig. 6, large errors occurred. It can be observed that when $T = 0.6$, the $angel$ and $bird$ produce the minimal error value of both RMSE and Metro. When $T = 0.7$, the $tubby$ and $duck$ meet the minimal error value of both RMSE and Metro. The best T can be slightly different for different modes. The results suggest this paper chose $T = 0.65$ in the remaining experiments.

Fig. 7 shows the results for the $tubby, buddha, bird$, $duck$, $angel$, $lobster$, $frog$ and $valve$ models in terms of 90% simplification rate by using QSim and SSim respectively. In all the cases it can be observed that both methods contain the major topology characteristics of the initial models. But careful observation shows that SSim is better than the QSim for all the models in retaining local details. For example, on the model $tubby$, the eye area and ears are retained better by SSim. For model $bird$, the face and neck are over smoothed by QSim, but the characteristics of face and neck are still preserved well by SSim. For model $buddha$, the hair and eyebrow are preserved better by SSim and the hair is removed completely by QSim. Table.1 shows the RMSE and Metro errors of SSim and QSim for all models. It can be observed that if the simplification rate increases, the RMSE and Metro errors become much larger for both QSim and SSim as expected. Even though, the errors for SSim are much lower than those of QSim. Fig. 8 shows snapshot of the small topological feature preservation in terms of 90% simplification rate, where the eye region on the $bird$ surface is preserved well with SSim, but the shape of eye is over smoothed by QSim. For the surface of the $buddha$, the hair is removed completely by QSim, but the outline of the curls is still preserved well by SSim. The nostril of the $frog$ is almost removed after QSim, but preserved well by SSim. All results show that SSim can preserve small topological features faithfully.

B. Registration

In this article, the registration algorithm FICP [23] and SoftICP [24] are selected due to their high accuracy. The registration results can be determined from the rotation angles, average and standard deviation of errors of RCs [24, 25]. Since the FICP and SoftICP algorithms require a good initialisation of camera motion parameters, this section reports results from relatively small motions. Fig. 9 shows the SoftICP and FICP registration results which are demonstrated by our algorithm and a comparative algorithm. It can be observed that SoftICP algorithm registers all images accurately when sampling rates $P = 95\%$ (it means 95% of vertices are removed) and $P = 10\%$ were chosen, which indicates that accurate registration of overlapping range images is feasible based on sampling. However, with $P = 5\%$, the inaccurate registration results occur to either the SoftICP algorithm or the FICP. This is because too few points can hardly characterise the geometry of the range images and thus pose the registration problem. From the experimental results, it can

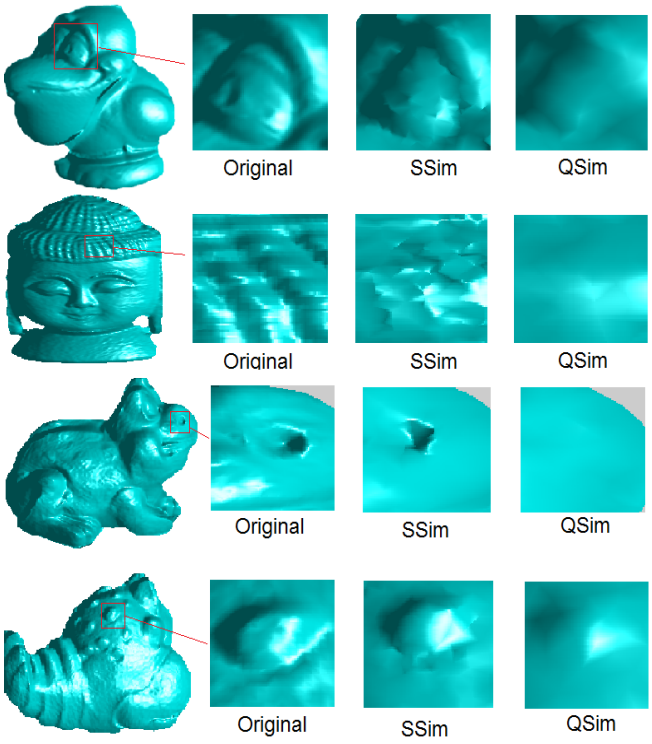

Figure. 8: Small topological feature preservation on bird, buddha, frog and lobster with 90% simplification rate

be seen that the SoftICP algorithm yields relatively stable results for each high quality image, and the FICP achieves a worse result than the SoftICP but it is still acceptable. In summary, the registration accuracy depends on how many points have been sampled. If the percentage of the sampled points is too small, a poor registration result may occur. The more points sampled, the higher accuracy achieved at the cost of longer time. If the range images are in low quality, all algorithms will perform poorly which suggests that more accurate and stable algorithms still need to be developed in future.

In this section, we perform a comparative study of the stratified points sampling (SPS) [19] algorithm and our algorithm (SBS). SPS method samples points independently from each part and generates evenly spaced samples by subdividing the sampling domain into non-overlapping parts. The algorithm is easily implemented and achieves good results. Experimental results are presented in Fig. 9. It can be seen that high percentage of data sampling often leads to an accuracy estimated rotation angle, yielding smaller average registration errors. It can also be seen that the SoftICP algorithm sometimes oscillates in the evolution of image registration. If the percentage of data sampling is between 95% to 10%, the estimated rotation angles decrease slowly. If the percentage of data sampling is below 10%, the estimated rotation angles are reduced more rapidly. This conclusion has been demonstrated by the experimental results while the FICP and SoftICP registration algorithms are implemented.

A careful analysis shows that our algorithm drops its performance more slowly than the SPS algorithm. For example, while the former performs very well even $P = 5\%$, the latter produces worse results even when P is as large as 10%. The evolution trend of the estimated rotation angle for registration based on the SPS algorithm is almost the same as our method: the fewer points sampled the smaller the estimated rotation angle. It is shown in Fig. 9(a) that our algorithm is significantly more accurate in the sense of average registration error over finally established point matches than SPS algorithm. For the FICP registration of the *tubby 1-2* when $P = 10\%$, SPS algorithm leads to an average registration error of 0.65mm and estimated rotation angle error is 3.2°, while the corresponding parameters for our algorithm are 0.3mm and 1.5° respectively. For the SoftICP registration of the *tubby 1-2*, the average registration error of the SPS sampled data is 0.32mm and estimated rotation error is 1.5°, while the corresponding parameters for our algorithm are 0.29mm and 0.6° respectively. It can be concluded that the SBS algorithm achieves higher accuracy than SPS algorithm in either SoftICP or FICP registration method. This is because the SPS algorithm has sampled the points independently from each part which is leading to sensitive to appearance and disappearance of points.

We evalute the computation time of the proposed algorithm and SPS algorithm in Fig. 9(d). Obviously, the computation time is reduced rapidly when the percentage of sampling drops. For the SoftICP registration on *tubby 1-2* when $P = 95\%$, our algorithm leads to a computation time that is *15s*, when $P = 5\%$, the computation time is *3s*. While the corresponding parameters for SPS algorithm are *17s* and *4s*. For the SoftICP registration on *buddha 1-2* when $P = 95\%$, our algorithm leads to a computation time is *23s*, when $P = 5\%$, the computation time is *3s*. While the corresponding parameters for SPS algorithm are *24.5s* and *4.5s*. It can be concluded that the SBS algorithm takes shorter computation time than SPS algorithm in either SoftICP or FICP registration method. Thus, we can say that the proposed method is more reasonable in terms of both accuracy and efficiency.

IV. Conclusions

This paper presents a novel approach to sample point from the input 3D data and the sampled points are representatively and distinctively. We propose a hybrid approach which combines mesh filtering, surface segmentation and point sampling. The proposed algorithm starts from a non-local mean filter on the shape index field in order to remove the noise. Then the segmentation approach combined with the Retinex method based on bilateral filtering for the illumination compensation of smoothed surface. Based on the segmentation regions, the points are selected by thresholding the shape index values. The method runs sufficiently quickly to be used as a preprocessing step to a variety of algorithms. The proposed sampling algorithm can detect the interest points according to the geometry and surface appearance information, and achieve the accurate registration and siplification results. The registration results show that when based on our method to sample points, it yields more accurate results using either SoftICP or FICP. The performances of simplification on various data show that our approach not only can represent the overall shape fidelity but also has the capability to retain the topology and small features well. The quality of images is vital to accurate segmentation, points sampling and image

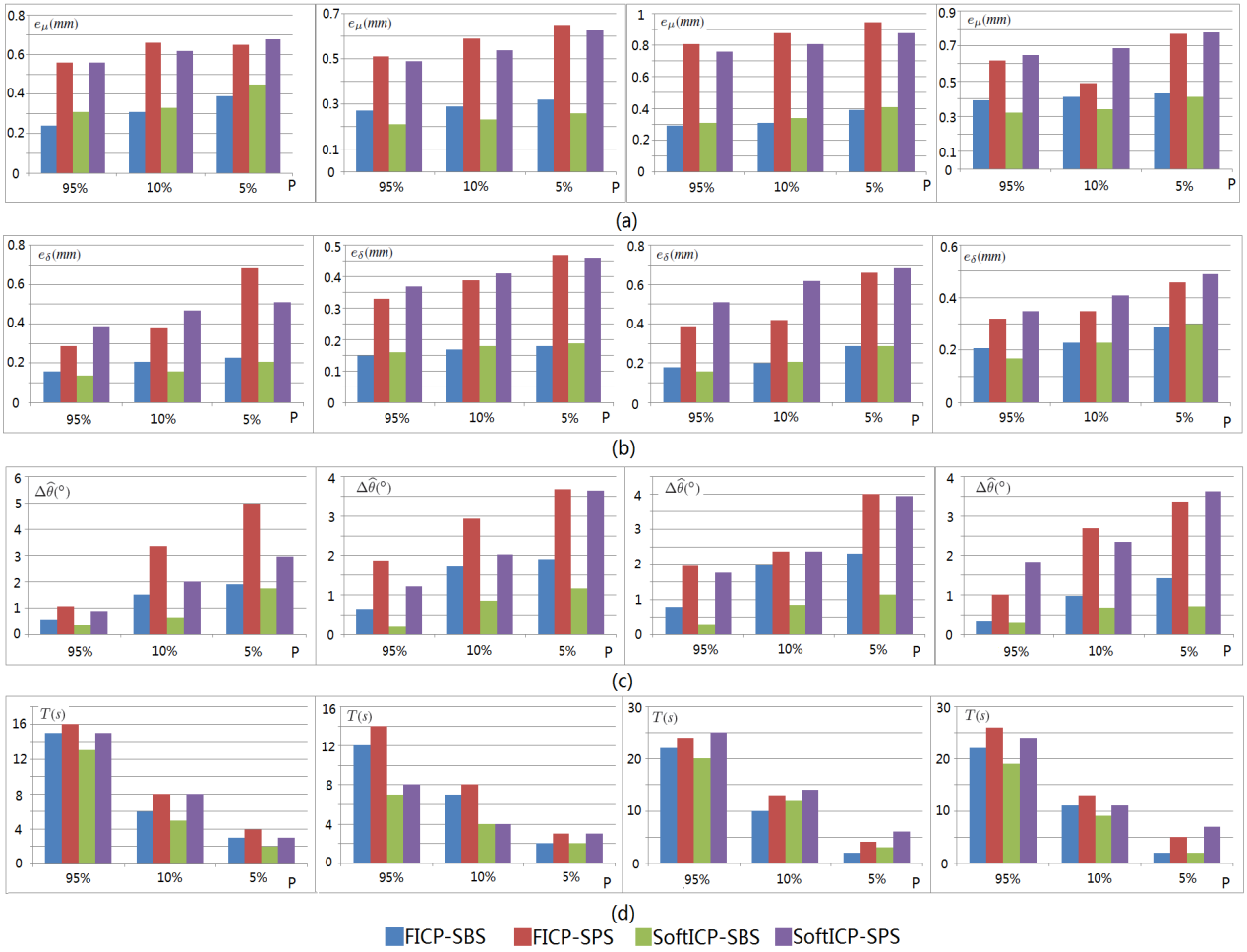

Figure. 9: The FICP and SoftICP registration results based on our method (SBS) and stratified points sampling method (SPS). Applied on several range images respectively. First row: tubby1-2; Second row: bird1-2; Third row: buddha1-2 and fourth row: duck1-2. The expected rotation is 20°. P is the percentage that sample points from the points cloud. (a) The average of registration errors e_{μ}. (b) The standard deviation of registration errors e_{δ}. (c) The calibrated rotation angle errors $\Delta\widehat{\theta}$. (d)Computation times in seconds for different algorithms.

registration. Directions for future work include improvement of the feature points extraction, saliency detection and design of appearance-preserving simplification.

V. Acknowledgements

We would like to thank Prof. Reyer Zwiggelaar and Zhili Chen from Aberystwyth University for their proofreading that has improved the readability of the paper.

References

[1] Y. Zhao, Y. Liu, R. Song and M. Zhang. A Retinex theory based points sampling method for mesh simplification, *7th International Symposium on Image and Signal Processing and Analysis*, pp. 230 - 235, 2011.

[2] Y. Zhao, Y. Liu, R. Song and M. Zhang. A Retinex theory based points sampling method, *3rd International Conference of Soft Computing and Pattern Recognition*, pp. 330 - 335, 2011.

[3] Y. Zhao, Y. Liu, R. Song and M. Zhang. A saliency detection based method for 3D surface simplification, *In Proc. 37th ICASSP*,to be appeared on March, 2012.

[4] C. Harris and M. Stephens. A combined corner and edge detector, *In Proc. of the 4th Alvey Vision Conference*, pp.147-151, 1988.

[5] J. Shi and C. Tomashi. Good feature to track, *In Proc. of IEEE Conf.on computer vision and pattern recognition*, pp. 593-600, 1994.

[6] D. Lowe. Distinctive image features from scale-invariant keypoints, *International Journal of computer vision*, 2004.

[7] A. Zaharescu, E. Boyer, K. Varanasi and R. Horaud. Surface feature detection and description with applications to mesh matching, *In Proc. CVPR*, 2009.

[8] T. Lo and J. Siebert. Local feature extraction and matching on range images: 2.5D SIFT, *Computer Vision and Image Understanding*, pp. 1235-1250, 2009.

[9] R. Osada, T. Funkhouser, B. Chazelle and D. Dobkin. Shape distributions, *ACM Transactions on Graphics*, 21(4), pp. 807-832, 2002.

[10] G. Turk. Re-tiling polygonal surfaces, *In Proc. of SIGGRAPH*, ACM press, 1992.

[11] M. Elad. Retinex by two bilateral filters, *In Proceedings of the Scale-Space conference*, 3459, pp. 217C229, 2005.

[12] M. Elad, R. Kimmel, D. Shaked, and R. Keshet. Reduced complexity retinex algorithm via the variational approach, *J. Vis. Commun. Image R*, 14, pp. 369C388, 2003.

[13] P. Felzenszwalab. Efficient graph-based image segmentation, *IJCV*, 59(2), pp. 167C181, 2004.

[14] R. Gross and V. Brajovic. An image preprocessing algorithm for illumination invariant face recognition, *4th International Conference on Audio and Video Based Biometric Person Authentication*, pp.10-18, 2003.

[15] D. Jobson, Z. Rahman, and G. Woodell. A multiscale retinex for bridging the gap between color images and the human observation of scenes, *IEEE Trans.Image Process*, 6(7), pp. 965C976, 1997.

[16] D. Jobson, Z. Rahman, and G. Woodell. Properties and performance of a center/surround retinex, *IEEE Trans. Image Process*, 6(3), pp. 451C462, 1997.

[17] J. Koenderink. Solid shape, *MIT Press*, pp. 18-28. 1990.

[18] E. Land. An alternative technique for the computation of the designator in the retinex theory of color vision, *Proc. Natl. Acad. Sci*, 83, pp. 3078C3080, 1986.

[19] D. Nehab and P. Shilane. Stratified point sampling of 3d models, *In Proc. of the symposium on point-based graphics*, pp. 49C56, 2004.

[20] G. Taubin. Estimating the tensor of curvature of a surface from a polyhedral approximation, *ICCV*, 4(2), pp. 107C114, 1986.

[21] J. Vollmer. R. Mencl, and H. Muller. Improved laplacian smoothing of noisy surface meshes, *Eurographics*, 18(3), pp. 111C117, 1999.

[22] J. Wu and L. Kobbelt. A stream algorithm for the decimation of massive meshes, *Graphics Interface*, pp. 185C192, 2003.

[23] J. Phillips, R. Liu and C. Tomasi. Outlier Robust ICP for Minimizing Fractional RMSD, *3-D Digital Imaging and Modeling*, pp.427-434, 2007.

[24] Y. Liu. Automatic 3d free form shape matching using the graduated assignment algorithm, *Pattern Recognition*, 38(10), pp.1615-1631, 2005.

[25] Y. Liu and B. Wei. Developing structural constraints for accurate registration of overlapping range images, *in Proc.Robotics and Autonomous Systems*, 47, pp.11-30, 2004.

[26] D. Huber and M. Hebert. Fully automatic registration of multiple 3D data sets,*IVC*, 21, pp.637-650, 2003.

[27] H. Chui and A. Rangarajan. A new point matching algorithm for nonrigid registration, *Comput. Vision Image Understand*, 89, pp.114-141, 2003.

[28] L. Itti, C. Koch, and E. Niebur. A model of saliency-based visual attention for rapid scene analysis, *PAMI*, pp. 1254-1259, 1998.

[29] Y. Hu, X. Xie, W. Ma, L. Chia, and D. Rajan. Salient region detection using weighted feature maps based on the human visual attention model, *Springer Lecture Notes in Computer Science*, pp. 993-1000, 2004.

[30] C. Lee, A. Varshney and D. Jacobs. Mesh saliency,*In ACM SIGGRAPH*, 2005.

[31] M. Pauly, R. Keiser and M. Gross. Multi-scale feature extraction on point-sampled surfaces, *Computer Graphics Forum* 22, 2003.

[32] P. Shilane and T. Funkhouser. Selecting distinctive 3D shape descriptors for similarity retrieval, *In SMI*, 2006.

[33] A. Frome, D. Huber, R. Kolluri, T. Bulow and J. Mailk. Recognizing objects in range data using regional point descriptors, *In ECCV*, 2004.

[34] Y. Kim and A. Varshney. Persuading visual attention through geometry,*IEEE Transactions on Visualization and Computer Graphics*, pp.772-82, 2008.

[35] Y. Miao, J. Feng and R. Pajarola. Visual saliency guided normal enhancement technique for 3D shape depiction, *Computers & Graphics*, pp.706-712,2011.

[36] A. Buades, B. Coll and JM. Morel. A non-local algorithm for image denoising, *In CVPR*, pp. 60-65, 2005.

[37] D.F. Rogers. An introduction to NURBS:with historical perspective, *Morgan Kaufmann*, pp. 179-181, 2001.

[38] P. Cignoni, C. Rocchini and R. Scopigno. Metro: measuring error on simplified surfaces, *Computer Graphics forum*,17(2), pp. 49-56, 1998.

[39] M. Garland and P. Heckbert. Surface simplification using quadric error metrics, *SIGGRAPH*, pp. 209-221, 1997.

[40] http://www2.ohio-state.osu.edu/data/3DDB/RID/index.htm

Author Biographies

Mr Yitian Zhao is a third year Ph.D. student at Department of Computer Science, Aberystwyth University, UK. He obtained his BEng in 2008 from the University of Central Lancashire, UK. He also acheived MSc in 2009 from Newcastle University, UK. So far, he has published three papers in international conference proceedings. His research interests lie in 3D data compression.

Dr Yonghuai Liu is a senior lecturer at Aberystwyth University. He obtained his first Ph.D. degree in 1998 from Northwestern Polytechnical University, PR China and his second Ph.D. degree in 2001 from The University of Hull, United Kingdom. From April to September 1999, he worked as a research assistant at the University of Hull. From March 2000 to September 2001, he worked as a research fellow at Sheffield Hallam University.

Dr Ran Songis currently a postdoctoral research associate with Department of Computer Science at Aberystwyth University, UK. He received his PhD degree from the University of York, UK and his first degree from Shandong University, China. His research interests lie in image registration, range image integration, surface reconstruction, etc.

Min Zhangis a third year PhD student at Aberystwyth University and a lecturer at Northwest University, China. She did her Master's Degrees in Literary Studies at Aberystwyth University and English Linguistics at Northwest University respectively and her Bachelor's in International Trade English with a second major in Computer Science.